Solid State Communications 337 (2021) 114440

Contents lists available at ScienceDirect

Solid State Communications

journal homepage: www.elsevier.com/locate/ssc

Vinyl chloride adsorption onto the surface of pristine, Al-, and Ga-doped boron nitride nanotube: A DFT study

Mohsen Doust Mohammadi [a], Hewa Y. Abdullah [b,*]

[a] School of Chemistry, College of Science, University of Tehran, Tehran, 14176, Iran
[b] Physics Education Department, Faculty of Education, Tishk International University, 44001, Erbil, Iraq

ARTICLE INFO

Communicated by T. Kimura

Keywords:
Boron nitride nanotube
Natural bond orbital
NCI
VCM
Vinyl chloride

ABSTRACT

The density functional techniques (DFT) were put into practice to study the nature of the intermolecular interactions between Vinyl chloride (VCM) gas molecule with single-walled pristine, Al and Ga-doped boron nitride nanotubes (BNNT, BNAlNT, and BNGaNT, respectively). For performing optimization process, various functionals including PBE0, M06–2X, ωB97XD, and B3LYP-D3 were applied on both of the isolated and complex structures. All of the functionals were used together with split-valence triple-zeta basis sets with d-type Cartesian-Gaussian polarization functions (6-311G(d)). To consider the electronic structure, total density of state (DOS) analysis were employed. Natural bond orbital (NBO), quantum theory of atoms in molecules (QTAIM), and non-covalent interaction (NCI) analyses were also taken on board to discover the nature of intermolecular interactions between gas and nanotubes. The results of electronic structure calculations as well as population analyses has been carefully tabulated and partially depicted. The HOMO-LUMO energy gap (HLG) were dramatically changed when the dopant atom added to the BNNT. It means the impurity can improve the sensivity and reactivity of the pristine nanotube; therefore, by absorbing the VCM onto the surface of the titled nanotubes, a salient signal can produce in a typical electronic circuit. Among all of the absorbents, BNGaNT shows the most favorable material to design a nanosensor for the studied gas molecule.

1. Introduction

After the emergence of density functional theory (DFT) due to its high computational power for large molecules as well as its considerable accuracy and speed, a suitable framework was provided for the theoretical studies of chemical systems. Many scientists today use this method to understand the properties of chemical structures. Meanwhile, theoretical studies on nanoscale structures have found an extraordinary place in computational chemistry, and researchers have used numerous computational methods to study intermolecular interactions to design tools that have better accuracy and performance [1–5]. A variety of nanomaterials have been considered for the construction of sensors with high measurement accuracy, extreme insensitivity to temperature, very low response time, low production costs, and resistant to harsh environmental conditions [6–12].

Different of methods have been used in theoretical studies to improve the sensitivity of the adsorption process in nanomaterials such as metal doping [13–15], surface defect [16–18], transition metal decoration [19,20], etc. Impurities introduced to the nanomaterial wall change the energy gap, and also dramatically change its morphology. Lin et al. provides a comprehensive study on the effect of transition metal decoration to boron nitride nanotube [21]. Studies have shown that even the introduction of non-metals such as oxygen can activate the surface of nanomaterials [22]. Demonstrating the benefits of dopant element, we can point out that by reducing the electrical resistance, impurity-decorated nanomaterials can generate a stronger signal in the circuit. Therefore, compared to pure nanomaterials, it can be said that decorated nanomaterials have a higher efficiency [23]. Aluminum and gallium and germanium are the elements that have been widely used to activate the surface of nanotubes in theoretical studies [24–27].

Following the discovery of boron nitride nanotubes in 1994 by Rubio et al. [28] and its synthesis by Chopra et al., In 1995 [29,30], Deca et al., Interactions between (10,0) and (10, 5) nanotubes 5) reported with the drug molecule isoniazid (INH); they showed that the binding energy of INH to BNNT (5,5) was slightly more significant than BNNT (10,0) [31]. Mukhopadhyay et al. Showed that by adsorption of tryptophan (non-polar amino acid), sparic acid and arginine (polar amino acid) on BNNTs, a strong bonding energy between polar amino acids on the

* Corresponding author.
E-mail address: hewayaseen@gmail.com (H.Y. Abdullah).

https://doi.org/10.1016/j.ssc.2021.114440
Received 21 October 2020; Accepted 10 July 2021
Available online 19 July 2021

Table 1
The adsorption energies (E_{ads}) for VCM/nanotube complexes. All values are in eV and obtained from geometry optimization calculations using PBE0, CAM-B3LYP, M06–2X, ωB97XD, and B3LYP-D3 functional in combination with 6-311G(d) basis set.

Systems	PBE0	CAM-B3LYP	M06–2X	wB97XD	B3LYP-D3
VCM/BNNT	−0.110	−0.080	−0.168	−0.272	−0.298
VCM/BNAlNT	−0.550	−0.527	−0.689	−0.731	−0.793
VCM/BNGaNT	−0.619	−0.611	−0.807	−0.805	−0.843

surface of boron nitride nanotubes is being observed [32]. Peyghan et al. investigated the absorption and electrical structure of BNNT (6.0) imidazole molecule in gaseous and soluble phases. They found that imidazole adsorption had no significant effect on the electrical structure of BNNT [33]. Yang et al. performed the interaction between BNNTs with biological molecules using DFT calculations [34]. Anota et al. investigated the interaction between BNNT and metformin using DFT methods [35]. Recently, the interaction between the uracil molecule with BNNT (n, 0) has been investigated by Mirzai et al. [36]. After the widespread use of boron nitride nanotube, there are lots of theoretical

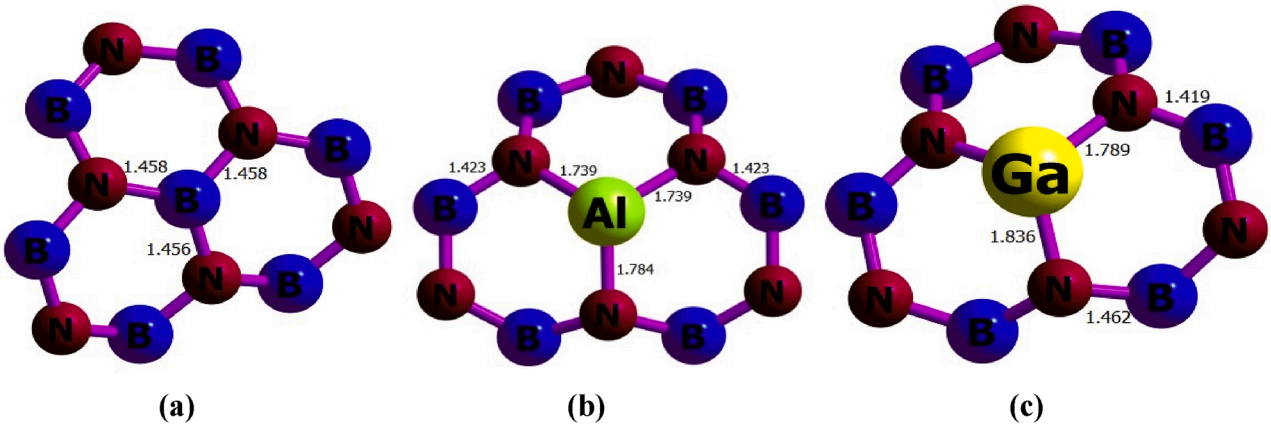

Fig. 1. The bond length (Å) obtained at ωB97XD/6-311G(d) level for **(a)** BNNT, **(b)** BNAlNT, and **(c)** BNGaNT.

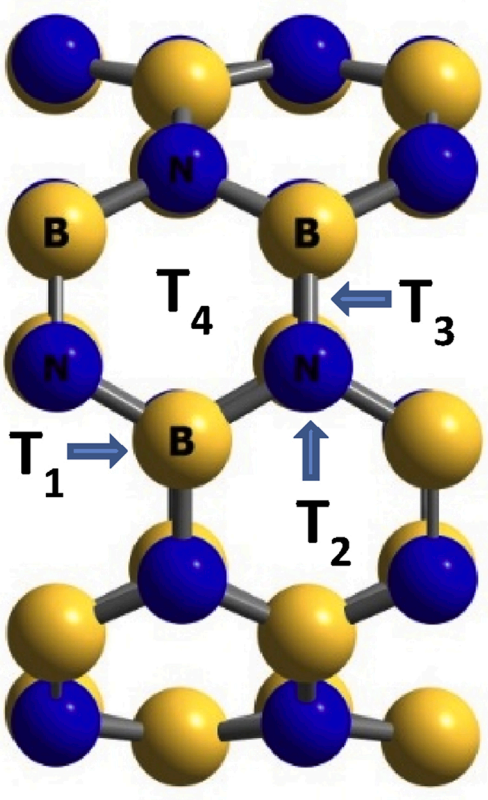

Fig. 2. The unit cells for BNNT prepared to perform one-dimensional periodic boundary condition density functional theory calculations. The T_x positions including on top of boron atom (T_1), on top of ntrogen atom (T_2), on top of the bond beween boron and notrogen atoms (T_3), and on top of the hexagonal ring (T_4).

investigation on the adsorption of different molecules onto the surface of different nanostructures like aluminun nitride, silicon carbid, etc [5,10–12,37–40].

This article encompasses a comprehensive study to investigate the intermolecular interactions of the VCM gas molecule with pristine BNNT plus nanotubes doped with Al and Ga elements. The details information about the computational level was given in section 2. The result and discussion section has been divided in 4 separate subsections: Geometric Surveys (3.1.), which provides insights about bond length and other geometry properties as well as introducing the levels of study for optimizing all structures; Electronic Structure (3.2.) that discusses about DOS and energetic properties results; NBO analysis (3.3.) and QTAIM analysis (3.4) are provided to show the nature of intermolecular

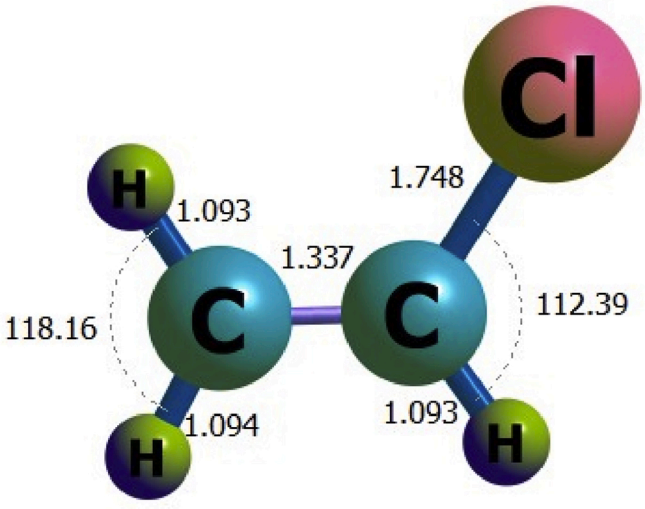

Fig. 3. The relaxed structure of the VCM gas molecule obtained from ωB97XD/6-311G(d) level of theory.

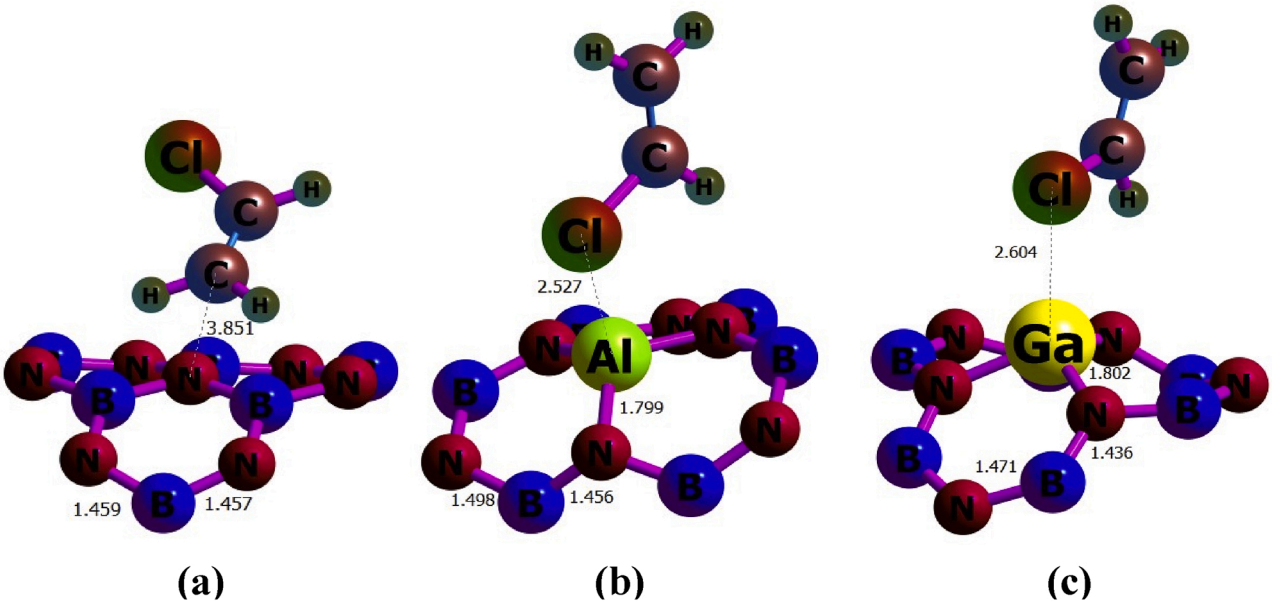

Fig. 4. The relaxed structures of a) VCM/BNNT, b) VCM/BNAlNT, and c) VCM/BNGaNT obtained from ωB97XD/6-311G(d) level of theory.

Table 2
HOMO energy (ϵ_H), LUMO energy (ϵ_L), Fermi energy (E_F), HOMO–LUMO energy gap (HLG), chemical potential (μ), chemical hardness (η), and electrophilicity (ω). All values are in eV and were obtained using the ωB97XD/6-311G(d) level of theory.

Systems	ϵ_H	ϵ_L	E_F	HLG	μ	η	ω
BNNT	−6.460	−0.183	−3.321	6.277	−3.321	3.139	17.312
BNAlNT	−6.330	−1.732	−4.031	4.598	−4.031	2.299	18.679
BNGaNT	−6.310	−2.390	−4.350	3.921	−4.350	1.960	18.547
VCM/BNNT	−6.413	−0.374	−3.394	6.039	−3.394	3.019	17.388
VCM/BNAlNT	−5.893	−1.397	−3.645	4.495	−3.645	2.248	14.931
VCM/BNGaNT	−5.749	−1.142	−3.445	3.607	−3.445	2.303	13.671

interactions between two fragments. We tried to provide a brief theory for each part using useful references and avoided to bring boring description. And finally, the conclusion section briefly refers to all the findings in this study.

2. Computational details

The PBE0 functional together with 6-311G(d) basis set were selected at the first stage to start the geometry optimization process of the isolated and complex structures. All of the structures were re-optimized using robust methods like M06–2X, ωB97XD, and B3LYP-D3. Head-Gordon et al. [41] invented the ωB97XD functional to account for the effect of long-range interactions as well as the dispersion corrections. Among Minnesota 06 suit, which is developed by Truhlar et al. [42], the global hybrid functional with double non-local exchange (2X) amounts (i.e. M06–2X) is a high performance method to study the non-covalent interactions. To study the dispersion effect, the latest version of B3LYP-D3 known as D3 (BD) (GD3BJ) developed by Grimme et al. [43–45] would be a good option. In order to compare the effect of each of the mentioned corrections, in Table 1, the amounts of adsorption energy obtained from ωB97XD method can be evaluated with other methods.

The PBC-DFT framework at PBE0/6-311G(d) level was applied on a pristine unit cell of $B_{40}N_{40}$ with 5.38 Å length(and 6.95 Å diameter). Re-optimization process were performed using 3 other functionals (M06–2X, ωB97XD, and B3LYP-D3) and same basis set. The values of bond length for BNNT, BNAlNT, and BNGaNT are depicted in Fig. 1. As is obvious from Fig. 1 (a), the B–N length are 1.46 Å. Also, Fig. 1 (b) and (c) show the value of bond length for Al–N and Ga–N 1.74 Å and 1.84 Å (and 1.79 Å), respectively. Due to the inner stress, the B–N bond length in the vicinity of Al and Ga dopant atoms are 1.42 Å.

The adsorption of VCM gas molecule onto the surface of BNNT, BNAlNT, and BNGaNT were also carried out. To achieve this goal, the gas molecule should be placed on top of the nanotube in different positions through different orientations. There are 4 different sites in the BNNT (Fig. 2) including on top of boron atom (T_1), on top of ntrogen atom (T_2), on top of the bond beween boron and notrogen atoms (T_3), and on top of the hexagonal ring (T_4). The purpose of such calculations is to find energy local minima. Fig. 3 shows the different heads of VCM including H and Cl heads. The gas molecule were put on top of each T_x sites through different distances and optimization process started at PM7/6-311G(d) level. It should be stressed that, overally, there are 80 initial orientations were prepared (i.e. $2 \times 4 \times 10 = 80$. It means 6 different gas molecule heads were put on each of the 4 sites of nanotube from 0.5 to 5.0 Å vertical distances with 0.5 Å intervals) for BNNT. Right after that, 6 minima were predicted for the gas/BNNT clusters. We select these 6 complex structures to optimize using PBE0/6-311G(d) level of theory. Regarding the values of adsorption energies, finally, the most stable complex were chosen and re-optimization were done using other functionals including M06–2X, ωB97XD, and B3LYP-D3. The relaxed structures of all complexes which has been obtained from ωB97XD/6-311G(d) are depicted in Fig. 4. When the values of E_{ads} are "below the range of chemical interest" [46], such results provides identical results.

The adsorption energy obtained from ωB97XD and B3LYP-D3 are closed to each other. The B3LYP-D3 functional shows the most negative E_{ads} values according to Table 1. It seems these two functional are good options for further investigations in this study. The most negative value of E_{ads} is corresponds to the adsorption of gas onto the BNGaNT,

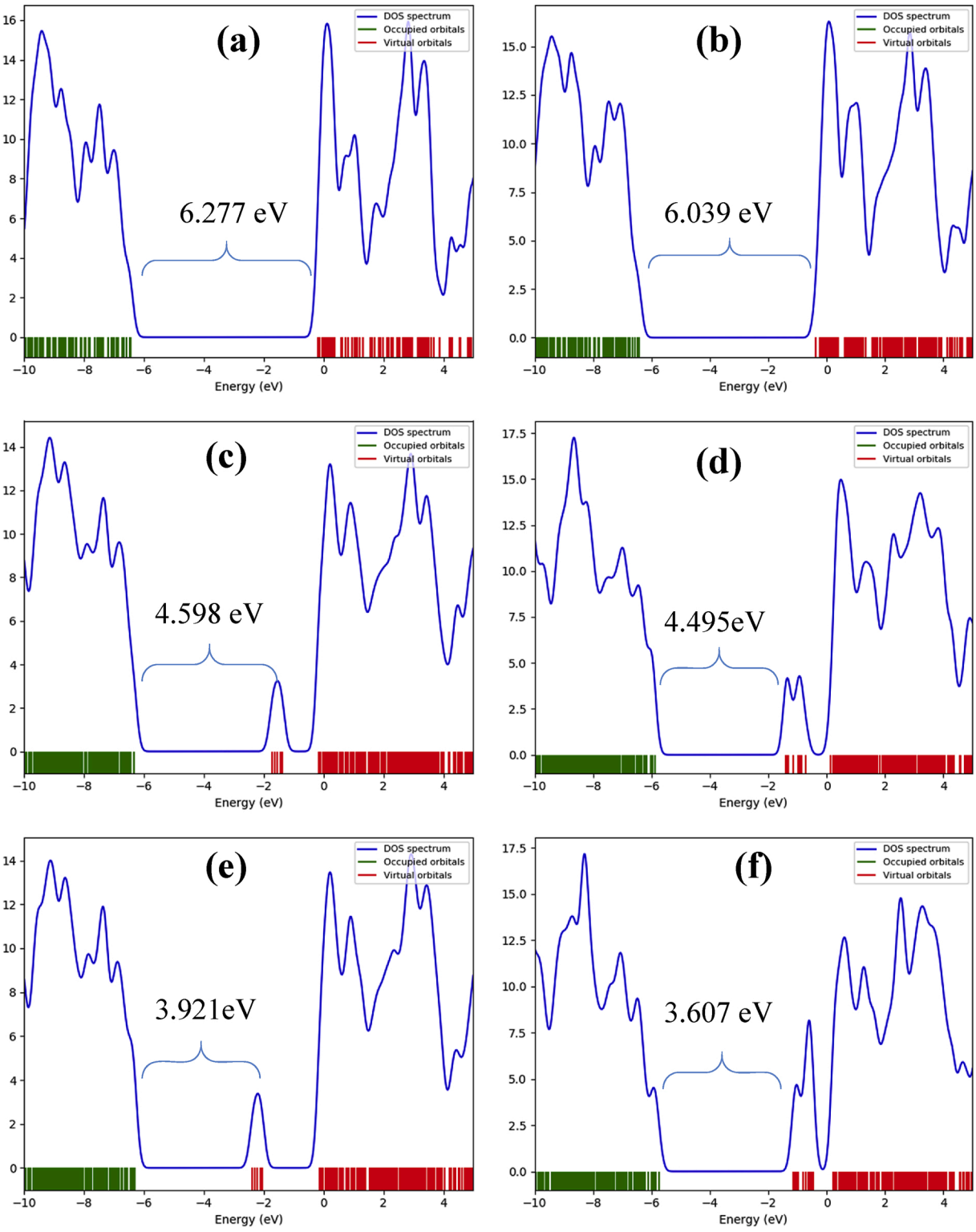

Fig. 5. Density of state maps for (a) BNNT (b) VCM/BNNT (c) BNAlNT (d) VCM/BNAlNT (e) BNGaNT (f) VCM/BNGaNT. Data were obtained from the ωB97XD/6-311G(d) level of theory.

−0.843eV which indicates that the reactivity of VCM gas is significant. Otherwise, the reactivity of gas and pristine BNNT shows the weakest interaction, among those nanotubes. We preferred to run the population analysis calculations with ωB97XD to reduce the computation times. Therefore, all the interactions analyses were applied to the results of the ωB97XD/6-311G(d) level of theory. For population analysis the unit cell expanded 5 times along with its centeral axis and calculations were performed. It should be noted that, to reduce the boundary effects, the terminal atoms were terminated by H atoms.

2.1. Electronic structure

The "Conceptual DFT" has been developed to consider the reactivity concept. Various properties can be obtained from HOMO-LUMO enrgy

Table 3
The values of Mulliken, Mayer, and Wiberg bond order obtained from the interactions of the VCM molecule with BNNT, BNAlNT, and BNGaNT. All calculations were performed using the ωB97XD/6-311G(d) level of theory.

Systems	X .....Y	Mulliken	Mayer	Wiberg
VCM/BNNT	Cl .....B	0.014	0.031	0.106
VCM/BNAlNT	Cl .....Al	0.105	0.264	0.481
VCM/BNGaNT	Cl ....Ga	0.131	0.291	0.598

(a) X atoms are belong to VCM.
(b) Y atoms are belong to nanotubes.

$$S = \left| \left(\frac{\sigma_1}{\sigma_2}\right) - 1 \right| = \exp\left(\frac{|\Delta E_g|}{kT}\right) - 1 \tag{7}$$

$$\sigma = AT^{3/2} e^{\frac{E_g}{2kT}} \tag{8}$$

Where A is a constant and σ is electrical conductivity, k is Boltzmann's constant, and T is Kelvin temperature. The resistivity will be diminished when E_g is being reduced, since the resistivity is proportional to the reciprocal of the conducting electron population. Hence, the resistivity for tube/gas adsorption is low and the electric current generated in the

Table 4
QTAIM topological parameters for electron density $\rho(\mathbf{r})$, Laplacian of electron density $\nabla^2\rho(\mathbf{r})$, kinetic electron density $G(\mathbf{r})$, potential electron density $V(\mathbf{r})$, bond ellipticity index (ε), and eta index (η)at the BCPs of the VCM clusters with BNNT, BNAlNT, and BNGaNT. All values were calculated using the ωB97XD/6-311G(d) level of theory and NBO analysis.

Systems	Bond	ρ	$\nabla^2 r$	$G(\mathbf{r})$	$V(\mathbf{r})$	$G(\mathbf{r})/V(\mathbf{r})$	ε	η
VCM/BNNT	C .....B	0.005	0.014	0.003	−0.002	1.372	3.047	0.156
	Cl .....B	0.002	0.008	0.002	−0.001	1.397	0.575	0.123
VCM/BNAlNT	Cl .....Al	0.027	0.077	0.023	−0.026	0.874	0.116	0.191
	C .....Al	0.013	0.038	0.009	−0.008	1.105	0.256	0.199
VCM/BNGaNT	Cl ....Ga	0.035	0.091	0.028	−0.033	0.844	0.025	0.203
	C .....Ga	0.017	0.049	0.012	−0.011	1.039	0.245	0.221

gap (HLG) [47] in such a way when an external potential apply to a system the energy, in the Hohenberg-Kohn theorems [48] context, changes as follows:

$$\Delta E \equiv E[N+\Delta N, v(\mathbf{r})+\Delta v(\mathbf{r})] - E[N, v(\mathbf{r})] = \left(\frac{\partial E}{\partial N}\right)_v \Delta N + \int \left(\frac{\delta E}{\delta v(\mathbf{r})}\right)_N \delta v(\mathbf{r}) d(\mathbf{r}) + \frac{1}{2!}\left\{ \left(\frac{\partial^2 E}{\partial N^2}\right)_v \Delta N^2 + 2 \times \int \left(\frac{\partial}{\partial N}\left(\frac{\delta E}{\partial v(\mathbf{r})}\right)_N\right)_v \Delta N \delta v(\mathbf{r}) + \int\int \left(\frac{\partial^2 E}{\partial v^2(\mathbf{r})}\right)_N \delta v(\mathbf{r}) \delta v(\mathbf{r}') d\mathbf{r} d\mathbf{r}' \right\} + \ldots \tag{3}$$

In the above Taylor expansion N is a global quantity and $\nu(\mathbf{r})$ is a local function. Each term has a specifict meaning in the chemical language as follows:

$$-\chi = \left(\frac{\partial E}{\partial N}\right)_v = \mu \cong \frac{(\varepsilon_{LUMO} + \varepsilon_{HOMO})}{2} \tag{4}$$

$$\eta = \left(\frac{\partial \mu}{\partial N}\right) = \frac{1}{2}\left(\frac{\partial^2 E}{\partial N^2}\right)_v = \frac{1}{2}(IP - EA) \tag{5}$$

$$\omega = \frac{\mu^2}{2\eta} \tag{6}$$

Equation (4) shows the nagative electronegativity (χ) which is equal to chemical potential (μ). Also the values of HOMO and LUMO are related to the ionization affinity and electron affinity, respectively. You can follow the other terms to reach to the Fukui function, response function, dual descriptor, etc through literature [49,50]. And Equation (6) is related to the electrophilicity index (ω). The values of these properties are listed in Table 2.

The energy gap (E_g) of BNNT has calculated about 6.277 eV at ωB97XD/6-311G (d) level of theory and the adsorption of VCM on it reduced the energy gap to 5.800 eV. The Al and Ga-doped nanotubes were also reduced the E_g values. Table 2 Shows the LUMO values were largely stabilized then the E_g has been reduced. The sensor response (S) is defined according to the following equations:

circuit will face the lowest resistance. Density of state (DOS) map is useful in intuitively revealing density of distribution of molecular orbitals in different energy regions, and gap is directly visible from this map (Fig. 5).

2.2. NBO analysis

The Natural bond orbital (NBO) method, developed by Weinhold et al. [51–53], is one of the most respectful population analyses and uses to calculate the distribution of electron density in bonds between atoms. The term NBO refers to a bonding orbital with the maximum electron density. A density matrix, calculated from DFT, as well as atomic charge, are used to define natural bonding orbitals. To complete the span of valance space in addition to bonding NBO (σ), we need an antibonding NBO (σ*) as follows:

$$\sigma_{AB} = C_A h_A + C_B h_B \tag{9}$$

$$\sigma^*_{AB} = C_A h_A - C_B h_B \tag{10}$$

where h_A and h_B are natural hybrid valance orbitals, C_A and C_B are the corresponding polarization coefficients. In the present study, NBO calculations were performed to figure out various types of bond order including Mulliken [54] (Equation (11)) and Mayer [55–57] (Equation (12)) bond order as well as Wiberg bond index (WBI) in Löwdin orthogonalized basis [58,59] (Equation (13)). Thus,

$$I_{AB} = \sum_i \eta_i \sum_{a\in A}\sum_{b\in B} 2C_{a,i}C_{b,i}S_{a,b} = 2\sum_{a\in A}\sum_{b\in B} P_{a,b}S_{a,b} \tag{11}$$

$$I_{AB} = I^{\alpha}_{AB} + I^{\beta}_{AB} = 2\sum_{a\in A}\sum_{b\in B}\left[(P^{\alpha}S)_{ba}(P^{\alpha}S)_{ab} + (P^{\beta}S)_{ba}(P^{\beta}S)_{ab}\right] \tag{12}$$

$$I_{AB} = \sum_{a\in A}\sum_{b\in B} P^2_{ab} \tag{13}$$

In the above Equations, P and S are density and overlap matrix, respectively. Mulliken and Mayer's bond orders are sensitive to the basis set, spacially for the basis set including diffuse functions. On the other hand, Wiberg bond order with respect to the two other is less basis set dependence. Table 3 reports the values of obtained bond orders from different methods. According to the WBI which is more accurate than Mayer and Mulliken we can up to this conclusion that BNAlNT and BNGaNT adsorbents are more active material in this study for adsorbing

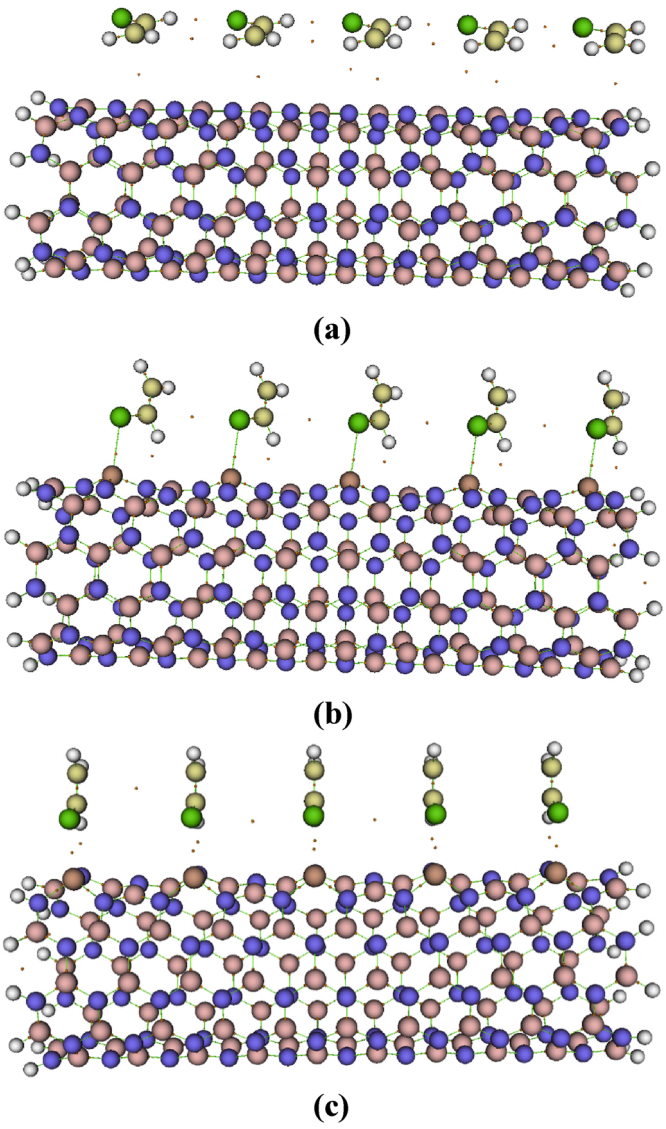

Fig. 6. The Bond critical points graphs for the (a) VCM/BNNT (b) VCM/BNAlNT (c) VCM/BNGaNT systems. The orange dots represent the BCPs.

VCM rather than pristine BNNT. The bond order value shows that the interaction of the gas molcule with BNNT can be classified as physisorption; otherwise, the interactions between Al and Ge-doped BNCNT with the gas are more strong van der Waals interactions.

2.3. QTAIM analysis

QTAIM analysis is used study bond types and intermolecular interactions. A critical point of the electron density, including minimum, maximum, or saddle point, can belong to: (1) *Atomic critical point* (ACP); (2) *bond critical point* (BCP); (3) *ring critical point* (RCP); and (4) *cage critical point* (CCP). The Electron density $\rho(\mathbf{r})$ and the Laplacian electron density $\nabla^2\rho(\mathbf{r})$ are playing important role in the QTAIM analysis since they determine the segmentation and identification of different types of chemical interactions. A bond critical point with negative values of Laplacian electron density and large values of electron density ($\rho(\mathbf{r}) > 10^{-1}$ a.u.) is defined as a covalent bond. On the other hand, the positive value of $\nabla^2\rho(\mathbf{r})$ designates that the interactions can be classified as of the non-substrate close-shell type (which include ionic and van der Waals interactions) [60].

The values of Lagrangian kinetic energy $G(\mathbf{r})$ and potential energy density $V(\mathbf{r})$ divulges the nature of the intermolecular interaction; therefore, the ratio of $G(\mathbf{r})/|V|(\mathbf{r})$ can be hired as an appropriate index in link classification. When $G(\mathbf{r})/|V|(\mathbf{r}) < 0.5$, the nature of the interaction is covalent, and if $G(\mathbf{r})/|V|(\mathbf{r}) > 1$, the interaction is non-covalent. For closed-shell interactions η index at BCP is less than 1 and increases with increasing covalent character [61]. Large values of elliptical bond (ϵ) represents an unstable structure and defined as follows [62]:

$$\varepsilon = \frac{\lambda_1}{\lambda_2} - 1 \ , |\lambda_1| > |\lambda_2| \tag{14}$$

According to virial theorem [63], a relationship exists between $G(\mathbf{r})$, $V(\mathbf{r})$, and $\nabla^2\rho(\mathbf{r})$ as follows:

$$\frac{1}{4}\nabla^2\rho(\mathbf{r}) = 2G(\mathbf{r}) + V(\mathbf{r}) \tag{15}$$

From Table 4 all values for $\nabla^2\rho(\mathbf{r})$ are positive. The B ….Cl interaction between gas and BNNT shows a value of $G(\mathbf{r})/|V|(\mathbf{r})$ higher than 1; therefore, for the case of BNNT and gas, the interactions are non-covalent. However, for doped BNNTs the values of $G(\mathbf{r})/|V|(\mathbf{r})$ are between 0.5 and 1. These results shows intermolecular interactions are classified as strong interactions. And finally the small values of ϵ and η show that these structures are stable. Fig. 6 are depicted to show the bond critical points between gas and nanotubes.

The results of QTAIM, in the previous section, showed that the interactions between VCM and nanotubes are non-covalent; hence, it is useful to check them by a non-covalent analysis. Reduced density gradient (RDG) and $\mathrm{sign}\lambda_2(r)\rho(r)$ are a pair of functions used in non-covalent interaction (NCI) [64] analysis which can be implemented to visualize the region and the type of weak interactions. RDG is defined as follows [64, 65]:

$$\mathrm{RDG} = \frac{1}{2(3\pi^2)^{\frac{1}{3}}} \frac{|\overline{\Delta\rho}(\mathbf{r})|}{\overline{\rho(\mathbf{r})}^{\frac{4}{3}}} \tag{16}$$

The two functions RDG and $\mathrm{sign}\lambda_2(\mathbf{r})\rho(\mathbf{r})$ can be plotted to define specific areas. In this case, non-covalent interactions will be identified. The points that indicate strong interactions are located in the $\mathrm{sign}\lambda_2(\mathbf{r})\rho(\mathbf{r}) < 0$ region. Relatively weak van der Waals interactions are found in the $\mathrm{sign}\lambda_2(\mathbf{r})\rho(\mathbf{r}) \approx 0$ region. And if points are in $\mathrm{sign}\lambda_2(\mathbf{r})\rho(\mathbf{r}) > 0$ region, it means that the interactions are of the type of repulsive [64, 65]. As it turns out, bond strength is closely related to the density matrix $\rho(\mathbf{r})$ as well as $\mathrm{sign}\lambda_2$. Low RDG and low electron density regions should be consulted to determine whether non-covalent interactions occur between the two components involved in the adsorption process.

Considering an isosurface as a reference (e.g. RDG = 0.5), it can be seen that the spots are appeared in the $\mathrm{sign}\lambda_2(r)\rho(r) \approx 0$ zone after the

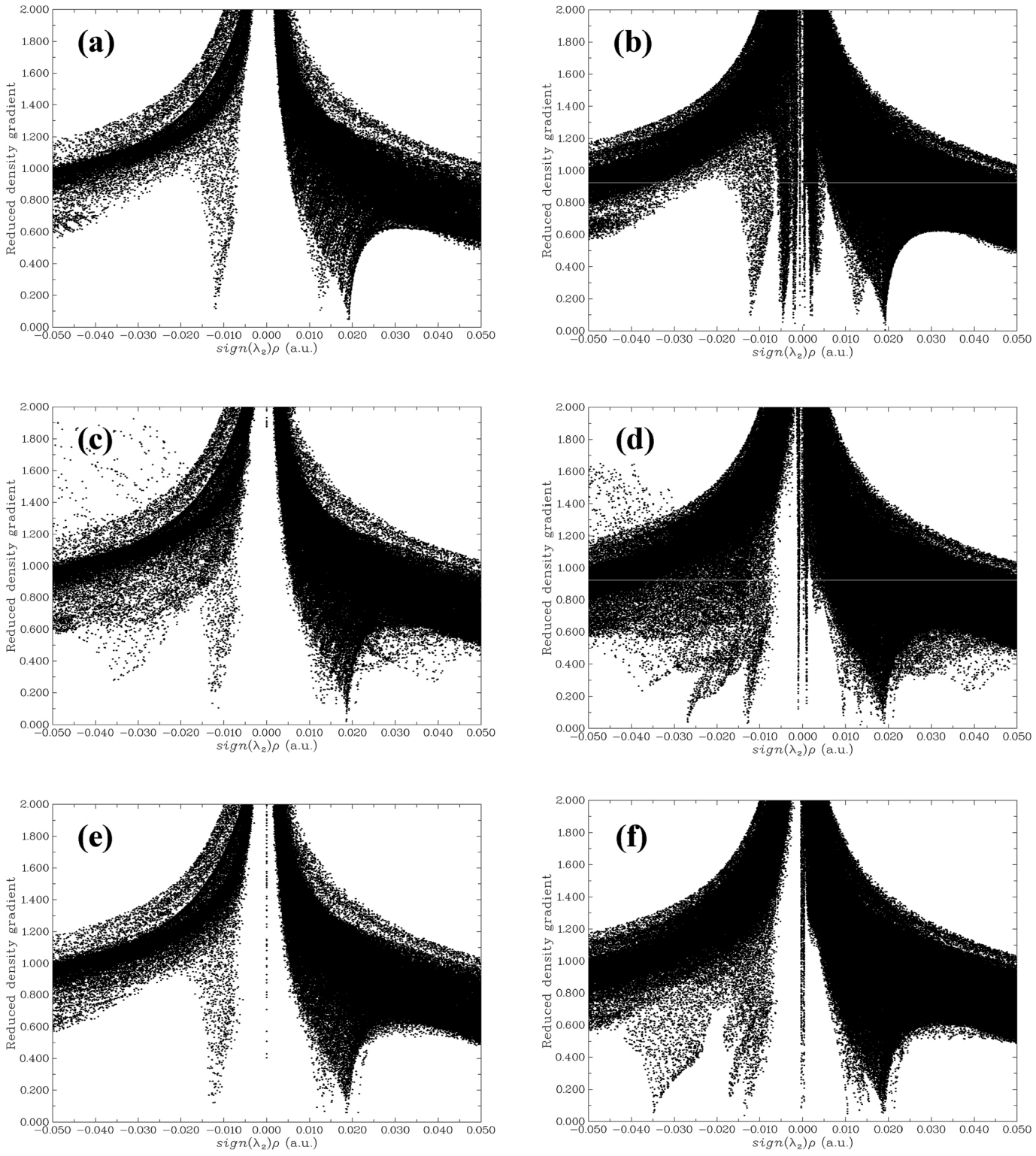

Fig. 7. The RDG (X-axis) vs. sign(λ_2)ρ(r) (Y-axis) diagrams (a) BNNT (b) VCM/BNNT (c) BNAlNT (d) VCM/BNAlNT (e) BNGaNT (f) VCM/BNGaNT. The diagrams were obtained from ωB97XD/6-311G(d) level of theory.

adsorption of gas molecule onto BNNT; therefore, the interactions can classified as van der Waals. However, the interactions of gas with-BNAlNT and BNGaNT were more stronger than BNNT in nature. NCI analysis also confirms the results of the adsorption energy calculations, QTAIM analysis, and NBO analysis, namely that the interactions of VCM with the doped nanotubes were strong (see Fig. 7).

3. Conclusion

The intermolecular interactions between the VCM gas molecule and BNNT, BNAlNT, and BNGaNT were studied by the DFT framework in vacuum condition. All molecular structures optimized at PBE0, ωB97XD, M06–2X, and B3LYP-D3 functionals together wit a 6-311G(d) basis set. Relaxed structures obtained from ωB97XD/6-311G(d) were chosen for

population analysis calculations. Results of adsorption energy show that among the nanotubes, the interaction of BNGaNT and gas (about −0.843 eV) is higher than the other adsorbents. Different bond order analysis data repeats former results. To shed light on the nature of intermolecular interactions NBO, QTAIM, and NCI analyses were implemented and the results of all the analyses were in agreement. From NBO analysis, the charge transfer was not observed and NCI and QTAIM results show van der Waals intermolecular interactions-specially for BNGaNT/gas cluster. To sum up, we can conclude injecting Al and Ga elements inside the BNNT can active its surface in favor of adsorbing VCM gas. Accordingly, this nanomaterial would be favorable for designing a sensitive nanosensor.

Declaration of competing interest

The authors declare that they have no known competing financial interests or personal relationships that could have appeared to influence the work reported in this paper.

Acknowledgements

I would like to thank the Solid-State Theory Group at the Physics Department at the Universita' degli Studi di Milano-Italy for providing computational facilities.

References

[1] M. Kamel, A. Morsali, H. Raissi, K. Mohammadifard, Theoretical insights into the intermolecular and mechanisms of covalent interaction of Flutamide drug with COOH and COCl functionalized carbon nanotubes: a DFT approach, Chemical Review and Letters 3 (2020) 23–37.
[2] R. Dos Santos, R. Rivelino, F. de Brito Mota, G. Gueorguiev, A. Kakanakova-Georgieva, Dopant species with Al–Si and N–Si bonding in the MOCVD of AlN implementing trimethylaluminum, ammonia and silane, J. Phys. Appl. Phys. 48 (2015) 295104.
[3] H. Ghafur Rauf, S. Majedi, E. Abdulkareem Mahmood, M. Sofi, Adsorption behavior of the Al-and Ga-doped B12N12 nanocages on COn (n= 1, 2) and HnX (n= 2, 3 and X= O, N): a comparative study, Chemical Review and Letters 2 (2019) 140–150.
[4] F. Li, H. Asadi, DFT study of the effect of platinum on the H2 gas sensing performance of ZnO nanotube: explaining the experimental observations, J. Mol. Liq. (2020) 113139.
[5] M.D. Mohammadi, M. Hamzehloo, The adsorption of bromomethane onto the exterior surface of aluminum nitride, boron nitride, carbon, and silicon carbide nanotubes: a PBC-DFT, NBO, and QTAIM study, Computational and Theoretical Chemistry 1144 (2018) 26–37.
[6] M.D. Mohammadi, H.Y. Abdullah, The adsorption of chlorofluoromethane on pristine, and Al-and Ga-doped boron nitride nanosheets: a DFT, NBO, and QTAIM study, J. Mol. Model. 26 (2020) 287.
[7] M.D. Mohammadi, H.Y. Abdullah, Theoretical study of the adsorption of amantadine on pristine, Al-, Ga-, P-, and As-doped boron nitride nanosheets: a PBC-DFT, NBO, and QTAIM study, Theoretical Chemistry Accounts 139 (2020) 1–17.
[8] M.D. Mohammadi, H.Y. Abdullah, The adsorption of bromochlorodifluoromethane on pristine and Ge-doped silicon carbide nanotube: a PBC-DFT, NBO, and QTAIM study, Structure. Chemistry 32 (2021) 481–494.
[9] M.D. Mohammadi, I.H. Salih, H.Y. Abdullah, An Ultimate Investigation on the adsorption of amantadine on pristine and decorated fullerenes C59X (X= Si, Ge, B, Al, Ga, N, P, and As): a DFT, NBO, and QTAIM Study, Journal of Computational Biophysics and Chemistry 20 (2020) 23–29.
[10] E. Nemati-Kande, M. Abbasi, M. Doust Mohammadi, DFT, QTAIM and NBO investigation of the interaction of rare gases with pristine and decorated boron nitride nanotube, Chemistry 3 (2018) 9833–9840.
[11] E. Nemati-Kande, M. Abbasi, M.D. Mohammadi, DFT studies on the interactions of pristine, Al and Ga-doped boron nitride nanosheets with CH3X (X= F, Cl and Br), J. Mol. Struct. 1199 (2020) 126962.
[12] E. Nemati-Kande, M. Abbasi, M.D. Mohammadi, Feasibility of pristine and decorated AlN and SiC nanotubes in sensing of noble gases: a DFT study, Chemistry 4 (2019) 2453–2462.
[13] K. Wilke, H. Breuer, The influence of transition metal doping on the physical and photocatalytic properties of titania, J. Photochem. Photobiol. Chem. 121 (1999) 49–53.
[14] J.A. Botas, G. Calleja, M. Sánchez-Sánchez, M.G. Orcajo, Cobalt doping of the MOF-5 framework and its effect on gas-adsorption properties, Langmuir 26 (2010) 5300–5303.
[15] D. Saha, S. Deng, Hydrogen adsorption on ordered mesoporous carbons doped with Pd, Pt, Ni, and Ru, Langmuir 25 (2009) 12550–12560.
[16] K. Bolton, A QM/MM study of HCl adsorption at ice surface defect sites, J. Mol. Struct.: THEOCHEM 632 (2003) 145–156.
[17] L.-Q. Wang, D.R. Baer, M.H. Engelhard, A.N. Shultz, The adsorption of liquid and vapor water on TiO2 (110) surfaces: the role of defects, Surf. Sci. 344 (1995) 237–250.
[18] Z. Wu, M. Li, J. Howe, H.M. Meyer III, S.H. Overbury, Probing defect sites on CeO2 nanocrystals with well-defined surface planes by Raman spectroscopy and O2 adsorption, Langmuir 26 (2010) 16595–16606.
[19] K. Srinivasu, S.K. Ghosh, Transition metal decorated porphyrin-like porous fullerene: promising materials for molecular hydrogen adsorption, J. Phys. Chem. C 116 (2012) 25184–25189.
[20] T. Yildirim, J. Íñiguez, S. Ciraci, Molecular and dissociative adsorption of multiple hydrogen molecules on transition metal decorated C 60, Phys. Rev. B 72 (2005) 153403.
[21] S. Lin, X. Ye, R.S. Johnson, H. Guo, First-principles investigations of metal (Cu, Ag, Au, Pt, Rh, Pd, Fe, Co, and Ir) doped hexagonal boron nitride nanosheets: stability and catalysis of CO oxidation, J. Phys. Chem. C 117 (2013) 17319–17326.
[22] W. Lei, H. Zhang, Y. Wu, B. Zhang, D. Liu, S. Qin, Z. Liu, L. Liu, Y. Ma, Y. Chen, Oxygen-doped boron nitride nanosheets with excellent performance in hydrogen storage, Nanomater. Energy 6 (2014) 219–224.
[23] M. Hjiri, L. El Mir, S. Leonardi, A. Pistone, L. Mavilia, G. Neri, Al-doped ZnO for highly sensitive CO gas sensors, Sensor. Actuator. B Chem. 196 (2014) 413–420.
[24] A.A. Darwish, M.M. Fadlallah, A. Badawi, A.A. Maarouf, Adsorption of sugars on Al-and Ga-doped boron nitride surfaces: a computational study, Appl. Surf. Sci. 377 (2016) 9–16.
[25] M.D. Esrafili, S. Asadollahi, A comparative DFT study on single-atom catalysis of CO oxidation over Al-and P-embedded hexagonal boron-nitride nanosheets, J. Mol. Graph. Model. 85 (2018) 323–330.
[26] A. Seif, K. Azizi, Charge-controlled switchable methane adsorption on heteroatom-doped BNNSs, RSC Adv. 6 (2016) 5079–5088.
[27] A. Seif, K. Azizi, A new strategy for hydrogen storage using BNNS: simultaneous effects of doping and charge modulation, RSC Adv. 6 (2016) 58458–58468.
[28] A. Rubio, J.L. Corkill, M.L. Cohen, Theory of graphitic boron nitride nanotubes, Phys. Rev. B 49 (1994) 5081.
[29] N.G. Chopra, L.X. Benedict, V.H. Crespi, M.L. Cohen, S.G. Louie, A. Zettl, Fully collapsed carbon nanotubes, Nature 377 (1995) 135–138.
[30] N.G. Chopra, R. Luyken, K. Cherrey, V.H. Crespi, M.L. Cohen, S.G. Louie, A. Zettl, Boron nitride nanotubes, Science 269 (1995) 966–967.
[31] N. Saikia, S.K. Pati, R.C. Deka, First principles calculation on the structure and electronic properties of BNNTs functionalized with isoniazid drug molecule, Appl. Nanosci. 2 (2012) 389–400.
[32] S. Mukhopadhyay, R.H. Scheicher, R. Pandey, S.P. Karna, Sensitivity of boron nitride nanotubes toward biomolecules of different polarities, J. Phys. Chem. Lett. 2 (2011) 2442–2447.
[33] A.A. Peyghan, M.T. Baei, M. Moghimi, S. Hashemian, Adsorption and electronic structure study of imidazole on (6, 0) zigzag single-walled boron nitride nanotube, J. Cluster Sci. 24 (2013) 31–47.
[34] C.-K. Yang, Exploring the interaction between the boron nitride nanotube and biological molecules, Comput. Phys. Commun. 182 (2011) 39–42.
[35] E.C. Anota, G.H. Cocoletzi, GGA-based analysis of the metformin adsorption on BN nanotubes, Phys. E Low-dimens. Syst. Nanostruct. 56 (2014) 134–140.
[36] M. Mirzaei, Uracil-functionalized ultra-small (n, 0) boron nitride nanotubes (n= 3–6), Computational studies, Superlattices and Microstructures 57 (2013) 44–50.
[37] M. Abbasi, E. Nemati-Kande, M.D. Mohammadi, Doping of the first row transition metals onto B12N12 nanocage: a DFT study, Computational and Theoretical Chemistry 1132 (2018) 1–11.
[38] Z. Mahdavifar, Z. Nomresaz, E. Shakerzadeh, Hetero-fullerenes C59M (M= B, Al, Ga, Ge, N, P, As) for sulfur dioxide gas sensing: computational approach, Chem. Phys. 530 (2020) 110606.
[39] N. Mohammadi-rad, M.D. Esrafili, J.J. Sardroodi, CuN3 doped graphene as an active electrocatalyst for oxygen reduction reaction in fuel cells: a DFT study, J. Mol. Graph. Model. (2020) 107537.
[40] E. Nemati-Kande, R. Karimian, V. Goodarzi, E. Ghazizadeh, Feasibility of pristine, Al-doped and Ga-doped Boron Nitride nanotubes for detecting SF4 gas: a DFT, NBO and QTAIM investigation, Appl. Surf. Sci. 510 (2020) 145490.
[41] J.-D. Chai, M. Head-Gordon, Long-range corrected hybrid density functionals with damped atom–atom dispersion corrections, Phys. Chem. Chem. Phys. 10 (2008) 6615–6620.
[42] F. Ma, Z.-R. Li, Z.-J. Zhou, D. Wu, Y. Li, Y.-F. Wang, Z.-S. Li, Modulated nonlinear optical responses and charge transfer transition in endohedral fullerene dimers Na@ C60C60@ F with n-fold covalent bond (n= 1, 2, 5, and 6) and long range ion bond, J. Phys. Chem. C 114 (2010) 11242–11247.
[43] S. Grimme, Semiempirical GGA-type density functional constructed with a long-range dispersion correction, J. Comput. Chem. 27 (2006) 1787–1799.
[44] S. Grimme, J. Antony, S. Ehrlich, H. Krieg, A consistent and accurate ab initio parametrization of density functional dispersion correction (DFT-D) for the 94 elements H-Pu, J. Chem. Phys. 132 (2010) 154104.
[45] S. Grimme, S. Ehrlich, L. Goerigk, Effect of the damping function in dispersion corrected density functional theory, J. Comput. Chem. 32 (2011) 1456–1465.
[46] J.B. Foresman, A. Frisch, Exploring Chemistry with Electronic Structure Methods: a Guide to Using Gaussian, 1996.
[47] J.-L. Bredas, Mind the gap!, Materials Horizons 1 (2014) 17–19.
[48] P. Hohenberg, W. Kohn, Inhomogeneous electron gas, Phys. Rev. 136 (1964) B864.
[49] P. Geerlings, F. De Proft, W. Langenaeker, Conceptual density functional theory, Chem. Rev. 103 (2003) 1793–1874.
[50] S.-B. Liu, Conceptual density functional theory and some recent developments, Acta Phys. Chim. Sin. 25 (2009) 590–600.

[51] a.J. Foster, F. Weinhold, Natural hybrid orbitals, J. Am. Chem. Soc. 102 (1980) 7211–7218.
[52] F. Weinhold, C.R. Landis, Natural bond orbitals and extensions of localized bonding concepts, Chem. Educ. Res. Pract. 2 (2001) 91–104.
[53] F. Weinhold, Discovering Chemistry with Natural Bond Orbitals, John Wiley & Sons2012.
[54] R.S. Mulliken, Electronic population analysis on LCAO–MO molecular wave functions. I, J. Chem. Phys. 23 (1955) 1833–1840.
[55] I. Mayer, Charge, bond order and valence in the AB initio SCF theory, Chem. Phys. Lett. 97 (1983) 270–274.
[56] I. Mayer, Improved definition of bond orders for correlated wave functions, Chem. Phys. Lett. 544 (2012) 83–86.
[57] A.J. Bridgeman, G. Cavigliasso, L.R. Ireland, J. Rothery, The Mayer bond order as a tool in inorganic chemistry, J. Chem. Soc., Dalton Trans. (2001) 2095–2108.
[58] K.B. Wiberg, Application of the pople-santry-segal CNDO method to the cyclopropylcarbinyl and cyclobutyl cation and to bicyclobutane, Tetrahedron 24 (1968) 1083–1096.
[59] O.V. Sizova, L.V. Skripnikov, A.Y. Sokolov, Symmetry decomposition of quantum chemical bond orders, J. Mol. Struct.: THEOCHEM 870 (2008) 1–9.
[60] C.F. Matta, Hydrogen–Hydrogen Bonding: the Non-electrostatic Limit of Closed-Shell Interaction between Two Hydro, Hydrogen Bonding—New Insights, Springer, 2006, pp. 337–375.
[61] B. Niepötter, R. Herbst-Irmer, D. Kratzert, P.P. Samuel, K.C. Mondal, H.W. Roesky, P. Jerabek, G. Frenking, D. Stalke, Experimental charge density study of a silylone, Angew. Chem. Int. Ed. 53 (2014) 2766–2770.
[62] H.J. Bohórquez, R.J. Boyd, C.F. Matta, Molecular model with quantum mechanical bonding information, J. Phys. Chem. 115 (2011) 12991–12997.
[63] S.J. Grabowski, QTAIM characteristics of halogen bond and related interactions, J. Phys. Chem. 116 (2012) 1838–1845.
[64] E.R. Johnson, S. Keinan, P. Mori-Sánchez, J. Contreras-García, A.J. Cohen, W. Yang, Revealing noncovalent interactions, J. Am. Chem. Soc. 132 (2010) 6498–6506.
[65] J. Contreras-García, E.R. Johnson, S. Keinan, R. Chaudret, J.-P. Piquemal, D. N. Beratan, W. Yang, NCIPLOT: a program for plotting noncovalent interaction regions, J. Chem. Theor. Comput. 7 (2011) 625–632.